Synthesis and gas sensing characteristics of highly crystalline ZnO–SnO$_2$ core–shell nanowires

In-Sung Hwang[a], Sun-Jung Kim[a], Joong-Ki Choi[a], Jaewan Choi[b], Hyunjin Ji[b], Gyu-Tae Kim[b], Guozhong Cao[c], Jong-Heun Lee[a,*]

[a] Department of Materials Science and Engineering, Korea University, Anam-Dong, Sungbuk-Gu, Seoul 136-713, Republic of Korea
[b] School of Electrical Engineering, Korea University, Seoul 136-713, Republic of Korea
[c] Department of Materials Science and Engineering, University of Washington, Seattle, WA 98195, USA

A B S T R A C T

The ZnO–SnO$_2$ core–shell nanowires (NWs) were synthesized by a continuous two-step vapor growth method at different synthesis temperatures. A crystalline 15–20 nm-thick, SnO$_2$ shell layer was pseudo-epitaxially coated on ZnO NWs with a diameter of 50–80 nm. The gas response of the ZnO–SnO$_2$ core–shell NW sensor to 10 ppm NO$_2$ reached ~33 times enhancement compared to that of the ZnO NWs at 200 °C. In addition, the ZnO–SnO$_2$ core–shell NW sensors showed selective detection to NO$_2$ at 200–300 °C and to C$_2$H$_5$OH at 400 °C. The enhanced gas responses to NO$_2$ and C$_2$H$_5$OH are discussed in relation to the thin SnO$_2$ shell layer and core–shell configuration of the NWs.

© 2010 Elsevier B.V. All rights reserved.

1. Introduction

One dimensional (1D) semiconductor nanowires (NWs) are an attractive material platform for gas sensor applications due to their large surface area, less agglomerated configuration and high crystallinity [1–4]. In particular, the gas response can be greatly enhanced when the diameter of 1D nanostructures becomes similar to the dimension of the electron depletion layer [5]. The formation of isolated functional layers on the surface of NWs using noble metals or metal oxides has also been studied to improve the gas responses and selectivity [6–8].

The formation of 1D heteronanostructures such as nanocomposite NWs or core–shell NWs can also be used to enhance the gas sensing characteristics. The electrospun SnO$_2$–ZnO composite nanofibers [9,10] have been reported to show high and selective responses to C$_2$H$_5$OH. Pulsed laser deposition and atomic layer deposition of a thin oxide shell layer on the electrospun core nanofibers or nanorods have been employed to prepare SnO$_2$–ZnO [11], TiO$_2$–ZnO [12] and ZnO–SnO$_2$ [13,14] core–shell 1D nanostructures. The α-Fe$_2$O$_3$–SnO$_2$ [15] and α-Fe$_2$O$_3$–ZnO [16] core–shell nanorods were also synthesized by hydrothermal preparation of nanorods and subsequent coating of the shell layer. These

showed the potential of hetero-nanostructures to enhance the sensing performance such as gas response and selectivity. However, the research in this field is in the beginning stage and further investigation is required to enhance and optimize the gas sensing characteristics.

In this contribution, crystalline ZnO–SnO$_2$ core–shell NWs were synthesized by a two-step vapor phase deposition method and their gas sensing characteristics were compared to those of ZnO NWs. The gas responses and selectivity to NO$_2$ and C$_2$H$_5$OH were enhanced significantly by the formation of a SnO$_2$ shell layer and the tuning of the sensor temperatures. The effect of the 15–20 nm-thick SnO$_2$ shell in improving the gas sensing characteristics is discussed in relation to the electron depletion of the shell layer and gas sensing mechanism of the hetero-nanostructures.

2. Experimental

The ZnO NWs were grown by carbothermal reduction process using ZnO and graphite powders in a horizontal furnace. The Si wafer coated with a 30 Å-thin Au layer was placed at the down-stream. After the quartz tube was evacuated to ~10^{-2} Torr using a rotary pump, Ar gas was introduced at a constant flow rate of 100 sccm. The furnace temperature was increased to 900 °C and O$_2$ gas with the flow rate of 2 sccm was introduced for 30 min. After the synthesis of single crystalline ZnO NWs, the furnace was cooled from 900 to 700 °C to deposit the SnO$_2$ shell layer. Tetramethyltin

---

* Corresponding author. Tel.: +82 2 3290 3282; fax: +82 2 928 3584.
  E-mail addresses: jongheun@korea.ac.kr, leejongheun@gmail.com (J.-H. Lee).

$((CH_3)_4Sn$, 99.999%, UP Chemical Co., Ltd.), one of the simplest organic tin compounds, was introduced into the quartz tube by Ar carrier gas at a flow rate of 0.5 sccm and reacted with an O_2 gas flow of 2 sccm for 10 min.

The morphology and structure of the ZnO–SnO_2 core–shell NWs were characterized with X-ray diffraction (XRD, Rigaku D/MAX-2500V/PC), field emission scanning electron microscopy (FESEM, Hitachi S-4300), transmission electron microscopy, energy-dispersive X-ray spectroscopy and selected area electron diffraction (TEM/EDX/SAED, JEOL JEM-3011).

The as-grown ZnO or ZnO–SnO_2 core–shell NWs were dispersed in a mixture of deionized water and isopropyl alcohol (IPA) (5:5 ml) by ultrasonication. The gas sensors were fabricated by depositing a slurry containing ZnO or ZnO–SnO_2 core–shell NWs on a poly-dimethylsiloxane (PDMS)-guided substrate. Subsequently, after drying and removal of the PDMS-guided layer, as-fabricated gas sensors were located at the sensing furnace and then heat-treated at 600 °C for 2 h in order to remove any residual organic contaminant. Detailed experimental procedures for sensor fabrication have been presented elsewhere [17]. The sensors were measured via a flow-through technique with a constant flow rate of 500 sccm at the gas sensing temperatures. The concentration of the target gas was controlled by changing the mixing ratio of the target gas and dry synthetic air.

3. Results and discussion

The SEM images and X-ray diffractions of as-grown ZnO NWs and SnO_2-coated ZnO NWs on Si substrate were shown in Fig. 1. The as-grown ZnO NWs were 50–80 nm-thick and several tens of micrometers long (Fig. 1(a)). After the deposition of SnO_2 for 10 min, the thickness was increased to 75–120 nm and the surface became rougher (Fig. 1(b)). The as-grown ZnO NWs were identified as hexagonal wurtzite ZnO (JCPDS #36-1451) from the XRD analysis results (Fig. 1(c)). In the SnO_2-coated ZnO NWs (Fig. 1(d)), rutile SnO_2 (JCPDS #41-1445) peaks were found, but no second phases such as SnO, $ZnSnO_3$ and Zn_2SnO_4 were observed.

The as-grown ZnO and SnO_2-coated ZnO NWs were separated from Si substrate and dispersed in a mixture of deionized water and IPA (5:5 ml) by ultrasonication. A slurry containing NWs after ultrasonic treatment was used both in TEM analysis and gas sensor fabrication. The ZnO NWs are single crystalline ones with clean surface morphology (Fig. 2(a)). After SnO_2 deposition, NWs with a core–shell configuration were obtained (Fig. 2(b)). High resolution TEM images show that the approximately 15 nm-thick crystalline shell layers were uniformly coated onto the ZnO NWs (Fig. 2(c)). Moiré patterns were clearly observed in the core region, having a wavy surface with a periodic range of about 3.7 nm (Fig. 2(b)), which was attributed to the overlapping of the different crystal lattices of ZnO and SnO_2. Two lattice planes with the interplanar distances of 0.52 and 0.48 nm correspond to the (0 0 0 1) plane of wurtzite ZnO and the (1 0 0) plane of rutile SnO_2, respectively (Fig. 2(c)). The SAED pattern for the region in Fig. 2(c) is shown in Fig. 2(d). The two sets of diffraction patterns, i.e. those for ZnO (red square) and SnO_2 (white square) were in agreement with the wurtzite ZnO $[2\bar{1}\bar{1}0]$ and rutile SnO_2 [1 0 0] zone axis patterns, respectively. The ZnO–SnO_2 nanostructure having a different crystal structure has been reported to reveal a special epitaxial relation [18]. The present SAED data support the epitaxial relationship that has been reported between a wurtzite ZnO core and a rutile SnO_2 shell, i.e. $(0\,1\,0)_{SnO2}\,\|\,(0\,\bar{1}\,1\,0)$ and $[1\,0\,0]_{SnO2}\,\|\,[0\,0\,0\,1]_{ZnO}$ [18]. However, the surface of SnO_2 shell layer was not completely smooth but locally rough. This suggests that some crystallites with the different orientations coexist. Therefore, the SnO_2 shell layer is thought to have a pseudo-epitaxial relationship with core ZnO NWs.
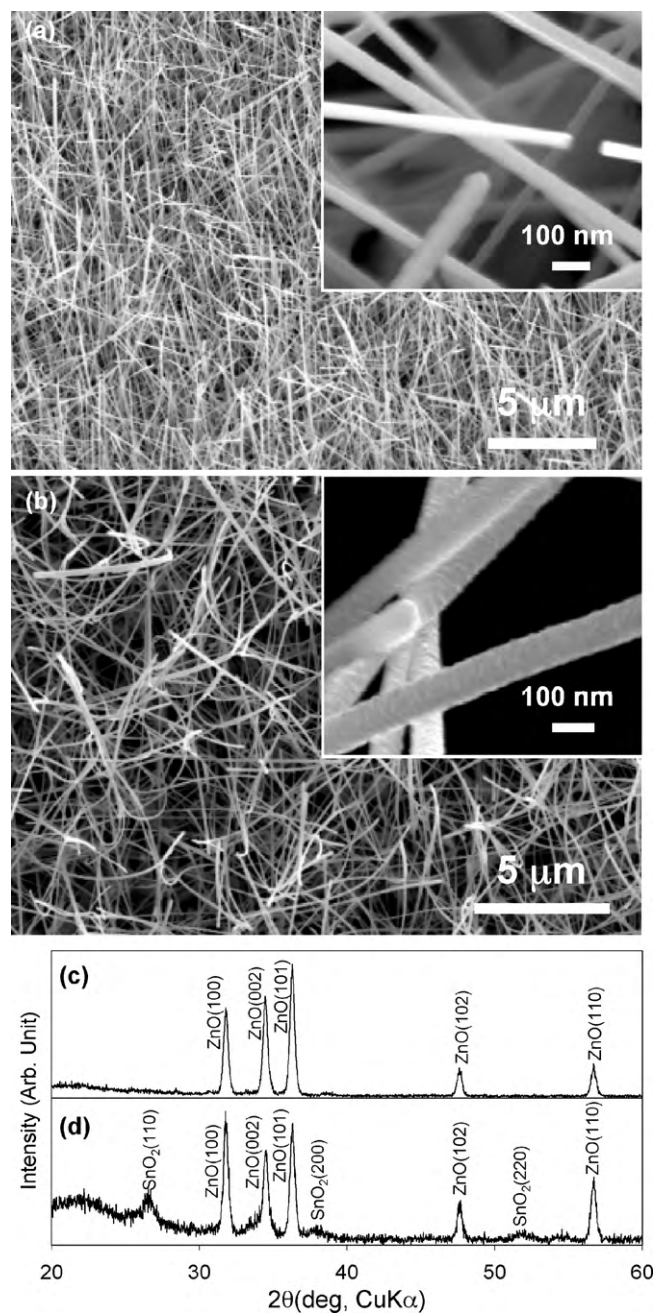
Fig. 1. Scanning electron microscopy (SEM) images and X-ray diffraction (XRD) patterns of as-grown ZnO NWs and ZnO–SnO_2 core–shell NWs: (a) SEM images of ZnO NWs, (b) SEM images of ZnO–SnO_2 core–shell NWs, (c) XRD pattern of ZnO NWs and (d) XRD patterns of ZnO–SnO_2 core–shell NWs.

The results of element mapping (Fig. 2(e and f)) clearly confirmed that the Sn elements were homogeneously distributed on the surface of the ZnO NWs. The presence of Sn, Zn and O elements within an individual NW was also confirmed by EDS analysis (data not shown). The above results demonstrate that ZnO–SnO_2 core–shell NWs can be synthesized successfully by pseudo-epitaxial deposition of crystalline SnO_2 shell layers on single crystalline ZnO NWs.

The gas sensing characteristics of ZnO and ZnO–SnO_2 core–shell NWs were investigated at sensing temperatures of 200 and 300 °C (Fig. 3). Note that ZnO and ZnO–SnO_2 core–shell NWs were heat-treated at 600 °C after sensor fabrication. However, considering that the heat treatment temperature is lower than the temperatures

for the growth of ZnO NWs (900 °C) and the subsequent deposition of SnO_2 shell layers (700 °C), the physico-chemical change of NWs during heat treatment can be regarded as small. Both sensors showed typical gas sensing behaviors of n-type semiconductor, i.e. the resistance increased upon exposure to oxidizing gases (NO_2) and decreased upon exposure to reducing gases. Accordingly, the gas responses to NO_2 and to reducing gases are defined as R_g/R_a and R_a/R_g (R_g: resistance in gas and R_a: resistance in air), respectively. The gas responses of ZnO–SnO_2 core–shell NWs to 10 ppm NO_2 at 200 and 300 °C were 66.3 and 12.4, respectively, which were ~33 and 8.9 times higher than the respective values of 2.0 and 1.4 for ZnO NWs. The gas responses to other reducing gases such as CO, C_3H_8, CH_4, H_2 and C_2H_5OH were negligible (1.0–1.9), which revealed the promising potential of the ZnO–SnO_2
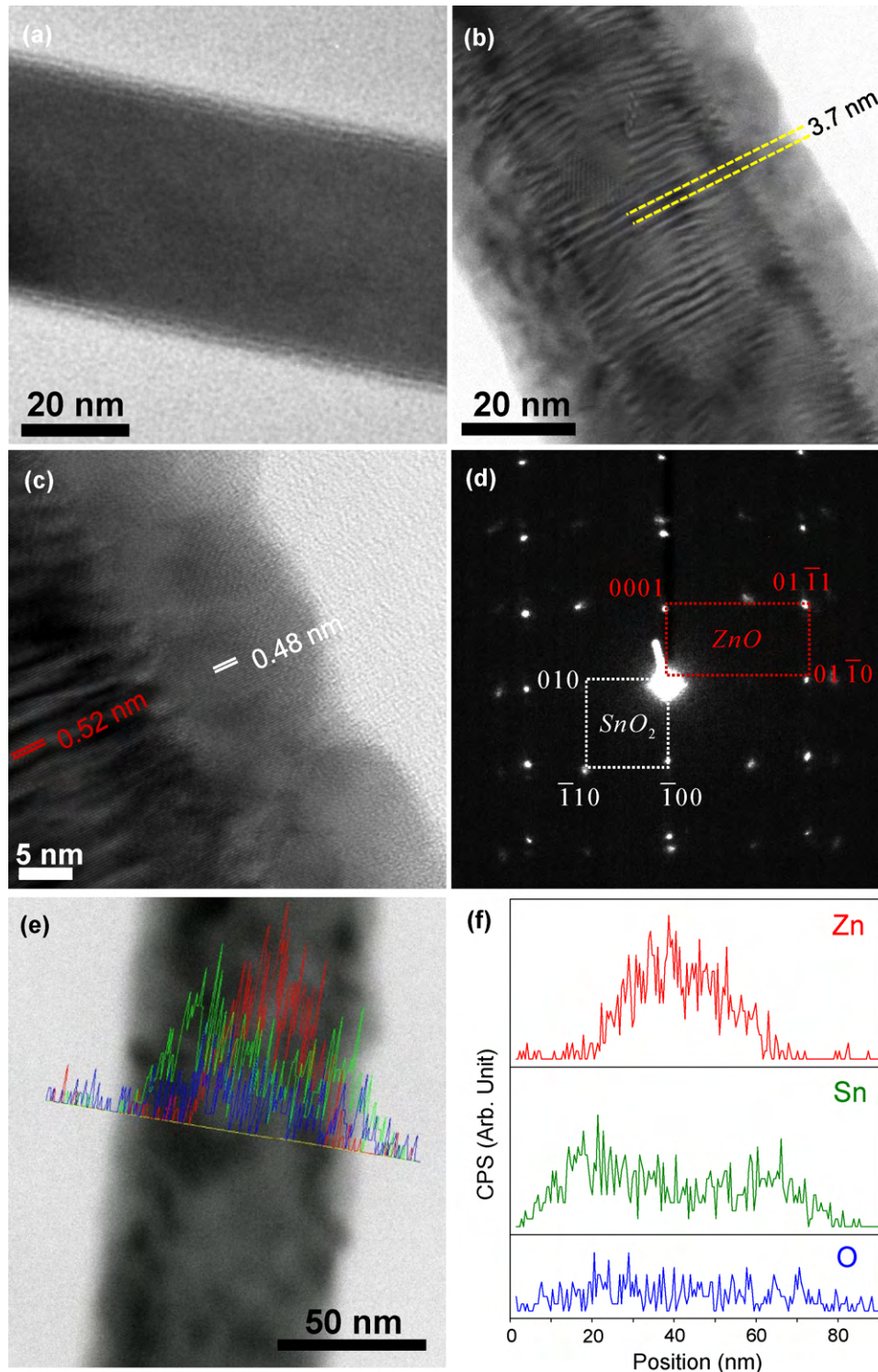
Fig. 2. (a) Transmission electron microscopy (TEM) image of ZnO NWs, (b and c) TEM images, (d) selected area diffraction pattern (SAED) of ZnO–SnO_2 core–shell NWs and (e and f) compositional analysis along a single ZnO–SnO_2 core–shell NW. The NWs were separated from Si substrate and subsequently dispersed in a mixture of deionized water and IPA by ultrasonic treatment to prepare TEM specimens.
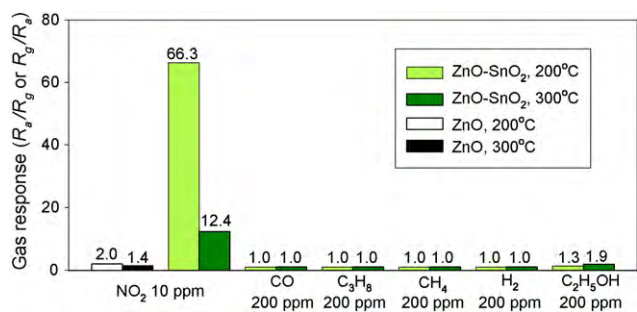
Fig. 3. Gas responses (R_g/R_a or R_a/R_g, R_a: resistance in air and R_g: resistance in gas) to 10 ppm NO_2 and 200 ppm of CO, C_3H_8, CH_4, H_2 and C_2H_5OH at 200 and 300 °C (R_g/R_a for NO_2 and R_a/R_g for other reducing gases).
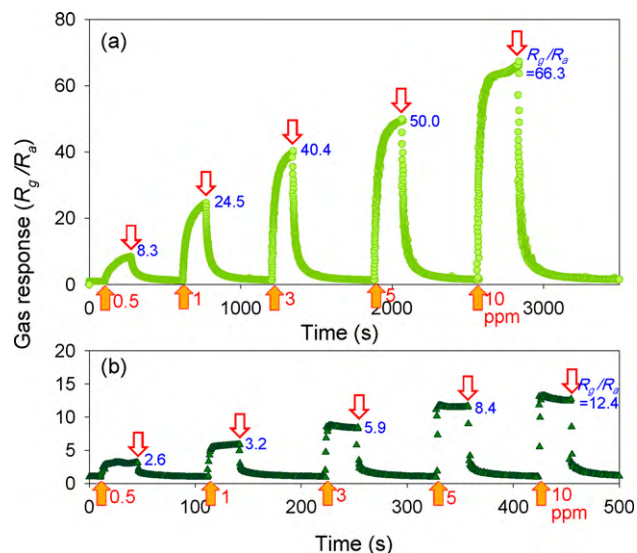
Fig. 4. NO_2 sensing transients of ZnO–SnO$_2$ core–shell NWs at (a) 200 °C and (b) 300 °C.

core–shell NWs for the sensitive and selective detection of NO_2 at 200–300 °C.

The NO_2 sensing transients of the ZnO–SnO$_2$ core–shell NWs at 200 and 300 °C are shown in Fig. 4. The gas responses to 0.5–10 ppm of NO_2 ranged from 8.3 to 66.3 at 200 °C, but were decreased to 2.6–12.4 as the sensor temperature was increased to 300 °C (Figs. 4 and 5(a)). The detection limits of NO_2 for ZnO–SnO$_2$ core–shell NWs were estimated to be approximately <15 and 138 ppb at 200 and 300 °C, respectively, when the criterion for gas

detection was set to $R_g/R_a > 1.2$. In contrast to the decrease of gas response, the speeds of gas response and recovery were greatly enhanced by the 100 °C increase in sensor temperature. To quantify this, the times to reach 90% variation in resistance upon exposure to NO_2 and air were defined as the 90% response (τ_{res}) and 90% recovery (τ_{recov}) times, respectively, and were calculated from the sensing transients in Fig. 4. The τ_{res} and τ_{recov} values to 0.5–10 ppm NO_2 were shortened by 15.8–65 and 5.0–11.4 times, respectively, as the sensor temperature was increased to 300 °C (Fig. 5(b and c)). This was attributed to the enhanced gas diffusion and the rate of surface reaction for gas sensing at the higher temperature. The operation of the sensor at 200 °C is advantageous for gas response and selectivity, whereas 300 °C is an attractive option for the rapid detection of NO_2 with moderate selectivity.

In the literature, the temperatures for maximum NO_2 response in SnO$_2$ and ZnO NWs (or nanobelts) sensors range from 200 to 225 °C [19–21], which agree well with the present results. Tamaki et al. [22] reported that the adsorbates originating from NO_2 are basically the same as those from NO because NO_2 is easily dissociated on the surface of SnO$_2$. Thus, the sensing of NO_2 at low operating temperatures is generally expressed by the chemisorptions of NO or NO_2 and consequent electron depletion according to the following reaction [20,23,24].

$$NO_2(g) + e^- \rightarrow NO_2^-(ads) \tag{1}$$

$$NO(g) + e^- \rightarrow NO^-(ads) \tag{2}$$

In any case, chemisorbed oxygen (O^- or O^{2-}) is not necessary in the gas sensing reaction. Thus, Baratto et al. [20] attributed the relatively low temperature for sensing NO_2 to the peculiar reaction mechanism of NO_2 with metal oxide that does not involve oxygen chemisorbed species. The maximum NO_2 response at 200 °C in the present study can be understood in the same viewpoint. The decrease of NO_2 response with increasing sensor temperature seems to be related to the desorption of NO_2^-(ads) at the higher temperature.

The variation of sensor temperatures not only changes the gas responding/recovery kinetics but also the selectivity in the gas sensing reaction [25,26]. Thus, the gas sensing characteristics of ZnO and ZnO–SnO$_2$ core–shell NWs at 400 °C were also investigated (Fig. 6). Interestingly, the response of the ZnO–SnO$_2$ core–shell NWs to 200 ppm C_2H_5OH was as high as 280, compared to a range from 2.3 to 16.2 for other gases (10 ppm of NO_2 and 200 ppm of CO, H_2, C_3H_8 and CH_4). In particular, the response to 10 ppm NO_2 became negligible (2.3) compared to those at 200 and 300 °C (66.3 and 12.4). This demonstrated the ability to detect C_2H_5OH with minimum interference from other gases by increasing the sensing temperature to 400 °C. The selective detection of 200 ppm C_2H_5OH was also
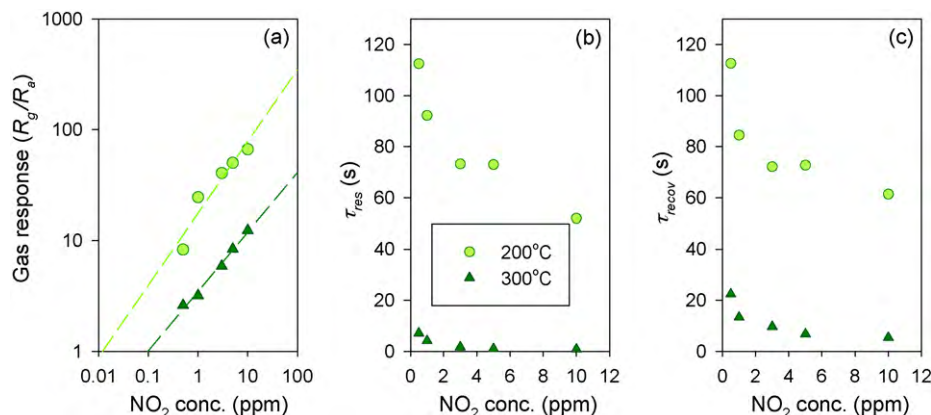
Fig. 5. (a) Gas responses (R_g/R_a), (b) 90% response time (τ_{res}) and (c) 90% recovery time (τ_{recov}) to 0.5–10 ppm NO_2 at 200 and 300 °C.
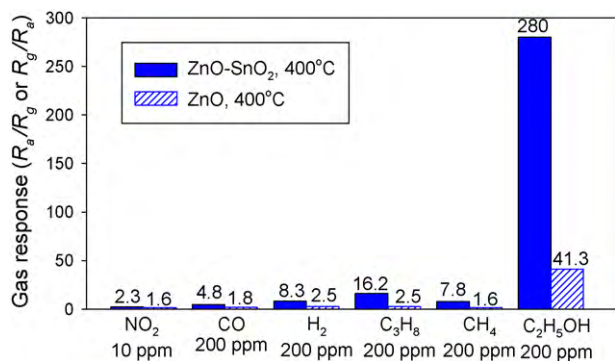
Fig. 6. Gas responses (R_g/R_a or R_a/R_g) to 10 ppm NO_2 and 200 ppm of CO, C_3H_8, CH_4, H_2 and C_2H_5OH at 400 °C (R_g/R_a for NO_2 and R_a/R_g for other reducing gases).

observed in ZnO NWs, but at a level of only 1/7 that of the ZnO–SnO$_2$ core–shell NWs (Fig. 6). This confirmed that the gas response and selectivity to C_2H_5OH can be enhanced by the formation of a SnO$_2$ shell layer and the tuning of the sensor temperatures.

The formation of a nanocomposite between SnO$_2$ and ZnO is known to increase the gas response and selectivity [9,10,27]. However, in the present study, SnO$_2$ shell layers were coated not in a discrete configuration but in a continuous and pseudo-epitaxial manner onto single crystalline ZnO NWs. Thus, the enhanced catalytic effect due to nanocomposite formation could be excluded in this study. The very high gas responses of the ZnO–SnO$_2$ core shell NWs to NO_2 and C_2H_5OH should therefore be understood in relation to the formation of thin SnO$_2$ shell layers.

In pure ZnO NWs at 200–400 °C, an electron depletion layer is formed near the surface by the adsorption of negatively charged oxygen (O^-), which increases the sensor resistance. Upon exposure to NO_2 or reducing gases, the surface becomes more resistive or conductive due to the reductive or oxidative interaction with gases, respectively. In this regard, the resistance variation of a single ZnO NW is determined by the parallel conduction along the resistive shell and semiconducting core and the resistive serial contact between NWs should be additionally taken into account in the networked ZnO NWs [17].

When a very thin SnO$_2$ layer is coated on the surface of ZnO NWs, the conduction mechanism becomes rather complex. Just after the formation of junction between SnO$_2$ and ZnO, the electrons will flow from the material with low work function to that with high work function until their Fermi levels equalize, which creates an electron depletion layer at the interface and bends the energy band. Unfortunately, the relative levels of work functions for SnO$_2$ and ZnO are not consistent in the literatures [28,29] and depend on the degree of nonstoichoiometry [30]. In any case, the formation of electron depletion layer in the vicinity of the interface due to the difference of work functions can be considered. The adsorption of negatively charged oxygen (O^-) at 200–400 °C at the surface of the shell SnO$_2$ layer forms another electron depletion layer near the surface. Barsan and Weimer [31] reported that the thicknesses of the electron depletion layer near the surface of the SnO$_2$ single crystal were 21 and 11 nm at 327 and 427 °C, respectively. Considering the 15–20 nm-thick SnO$_2$ shell layer in the present study, most of the SnO$_2$ shell layers were assumed to be fully depleted. Thus, the resistance of the networked ZnO–SnO$_2$ core–shell NWs was primarily determined by the fully depleted shell layer, the electron depletion layer at the interface between SnO$_2$ and ZnO, and the resistive contacts between NWs. The R_a values of ZnO NWs and ZnO–SnO$_2$ core–shell NWs at 200 °C are 96.7 and 730.7 kΩ, respectively. In the present study, the SnO$_2$ shell layers are coated completely and pseudo-epitaxially on the ZnO cores. Accordingly, this ~7-times greater resistance strongly supports the formation

of a highly resistive, electron-depleting, SnO$_2$ shell layer by the adsorption of negatively charged oxygen near the surface and the formation of an electron depletion layer at the interface between SnO$_2$ and ZnO. In this configuration, the resistance change upon gas exposure is primarily dependent upon the SnO$_2$ shell layers as well as the electron depletion layer at SnO$_2$–ZnO hetero-interface and is greatly increased. Thus, the significantly enhanced gas responses by the formation of the ZnO–SnO$_2$ core–shell NWs can be attributed to the nearly complete depletion of the SnO$_2$ shell layers.

4. Conclusion

The ZnO–SnO$_2$ core–shell nanowires (NWs) were synthesized via a two-step vapor growth method. After growth of single crystalline ZnO NWs by carbothermal reaction, a 10–15 nm-thick, SnO$_2$ crystalline layer was uniformly coated on the ZnO NWs by vapor phase reaction. The sensitive and selective detection of NO_2 and C_2H_5OH was achieved at 200 and 400 °C, respectively, with respective gas responses that were 33 and 6.8 times higher than those of the ZnO NWs. These enhanced gas sensing characteristics were attributed to the formation of a fully depleted thin SnO$_2$ shell layer and the electron depletion layer at SnO$_2$–ZnO interface.

References

[1] A. Kolmakov, M. Moskovits, Chemical sensing and catalysis by one-dimensional metal–oxided nanostructures, Annu. Rev. Mater. Res. 34 (2004) 151–180.
[2] E. Comini, C. Bratto, G. Faglia, M. Ferroni, A. Vomiero, G. Sberveglieri, Quasi-one dimensional metal oxide semiconductors: preparation and characterization and application as chemical sensors, Prog. Mater. Sci. 54 (2009) 1–67.
[3] D. Zhang, Z. Liu, C. Li, T. Tang, X. Liu, S. Han, B. Lei, C. Zhou, Detection of NO_2 down to ppb levels using individual and multiple In_2O_3 nanowire devices, Nano Lett. 4 (2004) 1919–1924.
[4] I.S. Hwang, E.B. Lee, S.J. Kim, J.K. Choi, J.H. Cha, H.J. Lee, B.K. Ju, J.H. Lee, Gas sensing properties of SnO$_2$ nanowires on micro heater, Sens. Actuators B., doi:10.1016/j.snb.2009.11.012, in press.
[5] Z. Fan, D. Wang, P.-C. Chang, W.-Y. Tseng, J.G. Lu, ZnO nanowires field effect transistor and oxygen sensing property, Appl. Phys. Lett. 85 (2004) 5923–5925.
[6] A. Kolmakov, D.O. Klenov, Y. Lilach, S. Stemmer, M. Moskovits, Enhanced gas sensing by individual SnO$_2$ nanowires and nanobelts functionalized with Pd catalyst particles, Nano Lett. 5 (2005) 667–673.
[7] N.V. Hieu, H.-R. Kim, B.-K. Ju, J.-H. Lee, Enhanced performance of SnO$_2$ nanowires ethanol sensor by functionalizing with La_2O_3, Sens. Actuators B 133 (2008) 228–234.
[8] I.-S. Hwang, J.-K. Choi, S.-J. Kim, K.-Y. Dong, J.-H. Kwon, B.-K. Ju, J.-H. Lee, Enhanced H_2S sensing characteristics of SnO$_2$ nanowires functionalized with CuO, Sens. Actuators B 142 (2009) 105–110.
[9] X. Song, Z. Wang, Y. Liu, C. Wang, L. Li, A highly sensitive ethanol sensor based on mesoporous ZnO–SnO$_2$ nanofibers, Nanotechnology 20 (2009) 075501.
[10] X. Song, L. Liu, Characterization of electrospun ZnO–SnO$_2$ nanofiber for ethanol sensor, Sens. Actuators A 154 (2009) 175–179.
[11] S.-W. Choi, J.Y. Park, S.S. Kim, Synthesis of SnO$_2$–ZnO core–shell nanofibers via a novel two-step process and their gas sensing properties, Nanotechnology 20 (2009) 465603.
[12] J.Y. Park, S.-W. Choi, J.-W. Lee, C. Lee, S.S. Kim, Synthesis and gas sensing properties of TiO$_2$–ZnO core–shell nanofibers, J. Am. Ceram. Soc. 92 (2009) 2551–2554.
[13] J.-A. Park, J.H. Moon, S.-J. Lee, S.H. Kim, H.Y. Chu, T.H. Zyung, SnO$_2$–ZnO hybrid nanofibers-based highly sensitive nitrogen dioxides sensor, Sens. Actuators B 145 (2010) 592–595.
[14] L.C. Tien, D.P. Norton, B.P. Gila, S.J. Pearton, H.-T. Wang, B.S. Kang, F. Ren, Detection of hydrogen with SnO$_2$-coated ZnO nanorods, Appl. Surf. Sci. 253 (2007) 4748–4752.
[15] Y.J. Chen, C.L. Zhu, L.J. Wang, P. Gao, M.S. Cao, X.-L. Shi, Synthesis and enhanced ethanol sensing characteristics of α-Fe_2O_3/SnO$_2$ core–shell nanorods, Nanotechnology 20 (2009) 045502.

[16] C.L. Zhu, Y.J. Chen, R.X. Wang, L.J. Wang, M.S. Cao, X.L. Shi, Synthesis and enhanced ethanol sensing properties of α-Fe_2O_3/ZnO heteronanostructures, Sens. Actuators B 140 (2009) 185–189.

[17] I.-S. Hwang, Y.-S. Kim, S.-J. Kim, B.-K. Ju, J.-H. Lee, A facile fabrication of semiconductor nanowires gas sensor using PDMS patterning and solution deposition, Sens. Actuators B 136 (2009) 224–229.

[18] Q. Kuang, Z.-Y. Jiang, Z.-X. Xie, S.-C. Lin, Z.-W. Lin, S.-Y. Xie, R.-B. Huang, L.-S. Zheng, Tailoring the optical property by a three-dimensional epitaxial heterostructure: a case of ZnO/SnO_2, J. Am. Chem. Soc. 127 (2005) 11777–11784.

[19] M.-W. Ahn, K.-S. Park, J.-H. Heo, J.-G. Park, D.-W. Kim, K.J. Choi, J.-H. Lee, S.-H. Hong, Gas sensing properties of defect-controlled ZnO-nanowire gas sensor, Appl. Phys. Lett. 93 (2008) 263103.

[20] C. Baratto, E. Comini, G. Faglia, G. Sberveglieri, M. Zha, A. Zappettini, Metal oxide nanocrystals for gas sensing, Sens. Actuators B 109 (2005) 2–6.

[21] Y.-J. Choi, I.-S. Hwang, J.-G. Park, K.J. Choi, J.-H. Park, J.-H. Lee, Novel fabrication of an SnO_2 nanowire gas sensor high sensitivity, Nanotechnology 19 (2008) 095508.

[22] J. Tamaki, M. Nagaishi, Y. Teraoka, N. Miura, N. Yamazoe, Adsorption behavior of CO and interfering gases, Surf. Sci. 221 (1998) 183–196.

[23] N. Yamazoe, K. Shimanoe, Theory of power laws for semiconductor gas sensors, Sens. Actuators B 128 (2008) 566–573.

[24] M. Epifani, J.D. Prades, E. Comini, E. Pellicer, M. Avella, P. Siciliano, G. Faglia, A. Cirera, R. Scotti, F. Morazzoni, J.R. Morante, The role of surface oxygen vacancies in the NO_2 sensing properties of SnO_2 nanocrystals, J. Phys. Chem. C 112 (2008) 19540–19546.

[25] A.P. Lee, B.J. Reedy, Temperature modulation in semiconducting gas sensing, Sens. Actuators B 60 (1990) 35–42.

[26] P. Heszler, R. Ionescu, E. Llobet, L.F. Reyes, J.M. Smulko, L.B. Kish, C.G. Granqvist, On the selectivity of nanostructured semiconductor gas sensors, Phys. Stat. Sol. B 244 (2007) 4331–4335.

[27] K.-W. Kim, P.-S. Cho, S.-J. Kim, J.-H. Lee, C.-Y. Kang, J.-S. Kim, S.-J. Yoon, The selective detection of C_2H_5OH using SnO_2–ZnO thin film gas sensors prepared by combinatorial solution deposition, Sens. Actuators B 123 (2007) 318–324.

[28] L. Zheng, Y. Zheng, C. Chen, Y. Zhan, X. Lin, Q. Zheng, K. Wei, J. Zhu, Network structured SnO_2/ZnO heterojunction nanocatalyst with high photocatalytic activity, Inorg. Chem. 48 (2009) 1819–1825.

[29] G. Mangamma, T. Gnanasekaran, Modeling of atmosphere sensitive heterojunctions for device applications, in: M. Laudon, B. Roamowicz (Eds.), Proceedings of 3rd International Conference on Modeling and Simulation of Microsystems, San Diego, CA, March 27–29, 2000, pp. 408–411.

[30] M. Batzill, U. Diebold, The surface and materials science of tin oxide, Prog. Surf. Sci. 79 (2005) 47–154.

[31] N. Barsan, U. Weimer, Conduction model of metal oxide gas sensors, J. Electroceram. 7 (2001) 143–167.

Biographies

In-Sung Hwang studied Materials Science and Engineering and received his BS from Kumoh National University, Korea, in 2004. In 2006, he received his MS degree from Korea University. He is currently studying for PhD at Korea University. His research interest is oxide nanostructure-based electronic devices.

Sun-Jung Kim studied Materials Science and Engineering and received his BS and MS degrees in 2006 and 2008, respectively, at Korea University in Korea. He is currently studying for PhD degree at Korea University. His research interests are oxide nanostructures for chemical sensor applications and the combinatorial design of gas sensing materials.

Joong-Ki Choi studied Materials Science and Engineering and received his BS degree from Korea University in 2009. He is currently a master course student at Korea University. His research topic is oxide nanowire gas sensors.

Jaewan Choi studied the Materials Science and received his BS from Hanyang University in 2005. He is currently in the course of PhD program at Korea University with a topic of the optoelectronic nanowire devices. His research interest covers the optoelectronic properties of the nanowire devices by realizing the intrinsic pn junctions in nanowires.

Hyunjin Ji studied the Electrical Engineering and received her BS from Korea University, Korea, in 2005. She is currently investigating the stability problems in nanowire devices as a PhD student. Her research interest includes the analysis of the electrical characteristics in nano-scale devices in detail for achieving the reproducible operation.

Gyu-Tae Kim has been a Professor at the School of Electrical Engineering, Korea University since 2002. He received his BS, MS and PhD degrees from the Department of Physics, Seoul National University in 1992, 1996 and 2000, respectively. Between 2000 and 2002, he investigated the electrical properties of nanostructures at the Max-Planck-Institute for Solid State Physics as a Humboldt Fellow. He developed a selective electron beam lithographic technique on a single nanowire and demonstrated the V_2O_5 nanowire FETs (Field Effect Transistors) for the first time as a nanowire electronic device. His current research interest covers the hybrid approaches in the nanotechnology for the educational and the research purposes.

Guozhong Cao is Boeing-Steiner Professor of Materials Science and Engineering at the University of Washington and received his PhD degree from Eindhoven University of Technology (The Netherlands), MS from Shanghai Institute of Ceramics and BS from East China University of Science and Technology (China). His recent research is focused mainly on synthesis and applications of nanomaterials for solar cells, lithium-ion batteries, catalysts and sensors.

Jong-Heun Lee joined the Department of Materials Science and Engineering at Korea University as an associate professor in 2003, where he is currently full professor. He received his BS, MS and PhD degrees from Seoul National University in 1987, 1989 and 1993, respectively. Between 1993 and 1999, he developed automotive air–fuel-ratio sensors at the Samsung Advanced Institute of Technology. He was a Science and Technology Agency of Japan (STA) fellow at the National Institute for Research in Inorganic Materials (currently NIMS, Japan) from 1999 to 2000 and a research professor at Seoul National University from 2000 to 2003. His current research interests include chemical sensors, functional nanostructures and solid oxide electrolytes.